

Evolution of coagulation-fragmentation stochastic processes using accurate chemical master equation approach

FARID MANUCHEHRFAR, WEI TIAN, TOM CHOU, AND JIE LIANG

Coagulation and fragmentation (CF) is a fundamental process in which smaller particles attach to each other to form larger clusters while existing clusters break up into smaller particles. It is a ubiquitous process that plays important roles in many physical and biological phenomena. CF is typically a stochastic process that often occurs in confined spaces with a limited number of available particles . Here, we study the CF process formulated with the discrete Chemical Master Equation (dCME). Using the newly developed Accurate Chemical Master Equation (ACME) method, we examine calculate the time-dependent behavior of the CF system. We investigate the effects of a number of important factors that influence the overall behavior of the system, including the dimensionality, the ratio of attachment to detachment rates among clusters, and the initial conditions. By comparing CF in one and three dimensions, we conclude that systems in three dimensions are more likely to form large clusters. We also demonstrate how the ratio of the attachment to detachment rates affects the dynamics and the steady-state of the system. Finally, we demonstrate the relationship between the formation of large clusters and the initial condition.

1. Introduction

Coagulation and fragmentation (CF) is a fundamental process in which particles attach to each other to form larger clusters that can also break down into smaller ones. The general mechanism presents itself in physical processes such as spray and aerosol [1–3], and biological processes such as filament formation and capsid protein nucleation [4, 5].

The CF process also lies at the heart of the blood clotting phenomenon [6–11]. The full coagulation cascade involves many molecular species and numerous reactions, often requiring complex models such as the ordinary differential equation (ODE) model of Hockin *et al.* (with 34 species and 42 rates) [12], or an even more complex platelet-plasma model of [13]. However, key steps involving the formation of cluster of fibrin particles can be regarded as a CF process [14].

The CF problem has been the focus of numerous theoretical and experimental studies [7, 15–17]. Theoretical approaches include Smolukowski's equation and the mass-action based Becker-Döring models [17, 19–21]. Solving these equations usually requires an assumption of infinite system size. However, CF often occurs in confined spaces with limited supply of molecules [17]. The behavior of CF in such small systems is intrinsically stochastic and the effects of the discreteness in particle and cluster numbers is significant.

The classic Becker-Döring-type models do not incorporate discreteness and stochasticity of the CF process [17, 22]. Instead, the Chemical Master Equation (CME) approach has been used to address the issue of discreteness and stochasticity [23–25]. Solution of the CME consists of a time-evolving probability landscape in state space, while the discrete form of the CME (dCME) can account for the finite size effects [26–28].

Monte Carlo (MC) simulation is commonly used to generate the trajectories from the discrete CME [29–32]. Studies based on MC simulations can incorporate both attachment and detachment reactions, discreteness, and can account for the stochasticity of the processes. However, they are limited by efficiency in sampling. To the best of our knowledge, there is no MC-based approach that can easily simulate the CF across all ranges of the attachment and detachment rates, in different dimensions, and starting with different initial conditions.

An alternative approach is to obtain an exact solution to the dCME. This is made possible by using the newly developed Accurate Chemical Master Equation (ACME) algorithm [33]. Using ACME, we first enumerate all the microstates reachable by the CF process from a given initial condition [34]. The transition matrix connecting these microstates are then calculated, which will be used to determine the time-evolution and steady-state of the probability landscape of the system. Using ACME, we examine how dimensionality of the system, the ratio of attachment to detachment rates among clusters, and the initial conditions affect the CF process.

2. Method

We first describe the CF process using the discrete Chemical Master Equation (dCME) [35]. In our system, there exists N molecular species n_1, n_2, \dots, n_N and m reactions with reaction rate constants r_1, r_2, \dots, r_m . The k -th reaction can be written as



The microstate of the system at time t can be represented by a vector of the copy number of each species: $x(t) = (x_1(t), x_2(t), \dots, x_N(t)) \in \mathbb{R}^N$, where $x_i(t)$ is the copy number of the i th specie at time t . The union of all possible microstates of the system across all times forms the state space S .

The rate of the k -th reaction that causes the transition of the system from the microstate j to the microstate i is defined as

$$(2) \quad A_k(x_i, x_j) \equiv r_k \prod_{z=1}^N \binom{x_z}{c_{z,k}}$$

The discrete Chemical Master Equation can be written as

$$(3) \quad \frac{\partial p(x, t)}{\partial t} = \sum [A(x, x')p(x', t) - A(x', x)p(x, t)]$$

Here, $p(x, t)$ is the probability to be at the microstate x , and $A(x, x')$ is the transition rate from microstate x' to microstate x . We obtain the probability $p(x, t)$ from Eq. (3) using the Accurate Chemical Master Equation (ACME) method [33].

In our finite-sized system, we assume that there is a source reservoir of particles, with a maximum capacity of M . Individual particles in the system can be generated through a reaction that produces clusters of size 1. Clusters of size 1 can also be removed by a degradation reaction, which deposits one particle back into the source reservoir. Furthermore, a cluster of size i and a cluster of size j can attach to each other and form a new cluster of size $(i + j)$, with the condition that $(i + j)$ cannot exceed a maximum cluster size of N . Clusters of size $(i + j)$ can also degrade into two clusters of size i and j via detachment reaction (see Fig. 1). Thus, we have four reactions of attachment, detachment, synthesis, and degradation (Eq. 4–7) in our CF system.

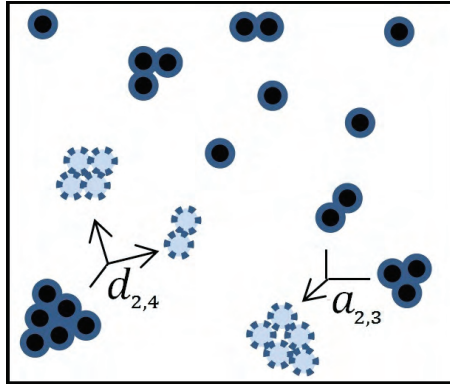
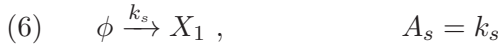
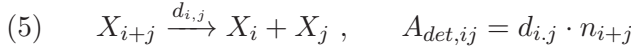


Figure 1: Schematic of a CF process illustrating possible steps of cluster attachment and fragmentation.

$$(4) \quad X_i + X_j \xrightarrow{a_{i,j}} X_{i+j}, \quad A_{att,ij} = \begin{cases} a_{i,j} \cdot n_i \cdot (n_j - 1)/2, & \text{if } i = j \\ a_{i,j} \cdot n_i \cdot n_j, & \text{if } i \neq j \end{cases}$$



Here, X_i represents a cluster of size i ; ϕ the source of the system; n_i the copy number of clusters of size i ; and $a_{i,j}/d_{i,j}$ the attachment/detachment rate constants, respectively. For one-dimensional systems, the clusters are linear chains of particles. The attachment and detachment of particles occur only at the ends of the cluster. Thus, the attachment and detachment rates are independent of the length of the cluster and will be taken to be constants. However, in two or three dimensions, both the attachment and detachment rates depend on the size of the clusters involved in the reaction. A simple model is that these rates depend on the perimeter and surface area of the clusters: $a_{i,j}, d_{i,j} \propto (i \cdot j)^{1/2}$ for two-dimensional systems, and $a_{i,j}, d_{i,j} \propto (i \cdot j)^{2/3}$ for three-dimensional systems [20].

To illustrate, we show a simple example in which we have the maximum cluster size $N = 3$ and the maximum total mass of the system $M = 4$. We assume that the system starts from the initial condition where there are four particles in the source and there is no cluster present in the system. In this simple system, we can have three different types of clusters, those of size 1, 2, and 3, respectively. Thus, each microstate of the system can be indexed

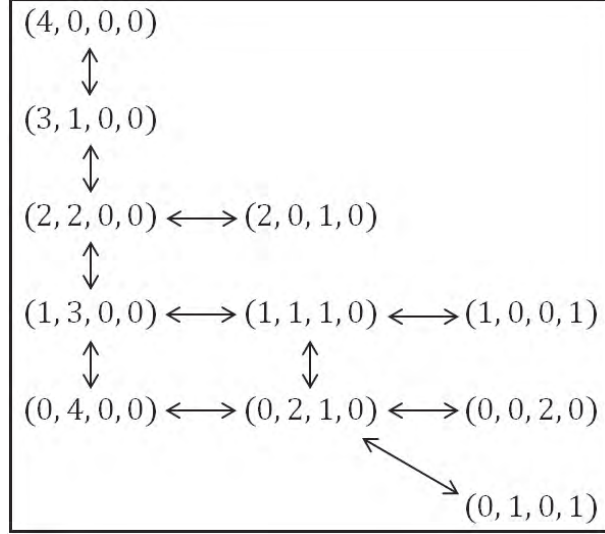


Figure 2: The state space of a system with a maximum cluster size $N = 3$ and total mass $M = 4$.

with four integers, the first indicating the number of particles in the source, and the second, third, and fourth integers indicating the number of clusters with size 1, 2, and 3, respectively. Eq. (8–10) are the reactions in this simple system, and the state space of the system is illustrated in Fig. 2.



We can then generate the rate matrix and calculate the probability of each microstate at the steady-state (Table 1). From the probability of each microstate, we can also find the expected number (Eq. 11) and the probability of each cluster (Eq. 12)

$$(11) \quad \langle n_i \rangle = \sum_i p_i \cdot n_i$$

$$(12) \quad P_{n_i} = \sum_i p_i (n_i \neq 0)$$

State index (i)	Prob. (ACME results)	State (source, n_1, n_2, n_3)
1	$p_1 = 1.97 \times 10^{-1}$	(4, 0, 0, 0)
2	$p_2 = 1.97 \times 10^{-1}$	(3, 1, 0, 0)
3	$p_3 = 9.84 \times 10^{-2}$	(2, 2, 0, 0)
4	$p_4 = 3.28 \times 10^{-2}$	(2, 0, 1, 0)
5	$p_5 = 8.20 \times 10^{-3}$	(1, 3, 0, 0)
6	$p_6 = 4.92 \times 10^{-2}$	(1, 1, 1, 0)
7	$p_7 = 9.84 \times 10^{-2}$	(1, 0, 0, 1)
8	$p_8 = 9.84 \times 10^{-2}$	(0, 4, 0, 0)
9	$p_9 = 9.84 \times 10^{-2}$	(0, 2, 1, 0)
10	$p_{10} = 9.84 \times 10^{-2}$	(0, 0, 2, 0)
11	$p_{11} = 2.46 \times 10^{-2}$	(0, 1, 0, 1)

Table 1: Steady-state probability of each microstate for example shown in Fig. 2

where i is the microstate index (Table 1), $\langle n_i \rangle$ the expected number of cluster of size i , and p_{n_i} the probability of observing a cluster of size i .

In our study, we restrict ourselves to a system with total mass of $M = 48$ and maximum possible cluster size of $N = 16$, which are much larger than those in previous studies ($M = 32$, $N = 8$) [30]. To describe the CF system, our state space contains $> 700,000$ microstates. For our calculations, we use a machine with a 20-core Xeon E5-2670 CPU of 2.5GHz, a cache size of 20MB, and 128GB RAM. Computing the steady-state distribution at each specific ratio of the attachment to detachment rates ($a_{i,j}/d_{i,j}$) takes about 38 minutes. Computing the time-evolving probability distribution takes between 2,729 minutes and 3,292 minutes. Table 2 provides details on the computational cost.

3. Results

Our results are organized as follows. We first examine the effect of dimensionality on the formation of the largest cluster in the system. We then study the effect of different ratios r of attachment/detachment rates $r = a_{i,j}/d_{i,j}$ on the formation of clusters and their steady-state distributions. Finally, we examine the effect of different initial conditions on CF dynamics.

$r = a_{ij}/d_{ij}$	Steady-state cost (min)	Time-evolving cost (min)
3.0	38	3,474
4.0	38	3,292
5.0	38	3,152
10.0	38	3,044
20.0	38	2,913
30.0	38	2,808
40.0	38	2,756
50.0	38	2,729

Table 2: Computational cost for computing the steady-state and time-evolving probability landscape of the system.

3.1. Effects of dimensionality

For one-dimensional systems, the attachment rate $a_{i,j}$ and the detachment rate $d_{i,j}$ are independent of the size of clusters. For two-dimensional and three-dimensional systems, we assume $a_{i,j}, d_{i,j} \propto (i \cdot j)^{1/2}$ and $a_{i,j}, d_{i,j} \propto (i \cdot j)^{2/3}$, respectively [20]. Fig. 3 compares probability of the largest clusters at different times when $r = 1.0$ in systems with different dimensionality.

There is a significant difference between the one-dimensional system and two-dimensional/three-dimensional systems. At long times, the probability of forming the largest clusters in three-dimensional systems is approximately twice that in one-dimensional systems. Since the difference in the large-cluster formation probabilities is negligible between two-dimensional and three-dimensional systems, we will examine the CF process in three dimensional systems for the rest of this paper.

3.2. Steady-state distributions

Expected number of clusters. Fig. 4A- 4D shows the expected number of clusters of different sizes for four different values of $r = 0.1, 1, 10$, and $1,000$ at the steady-state. When $r = 0.1$, most of clusters are singletons. When r increases, larger clusters form. When $r \approx 1,000$, all clusters are at their maximum allowed size. The expected number of all clusters at different ratios of attachment to detachment rates is shown in Fig. 4E.

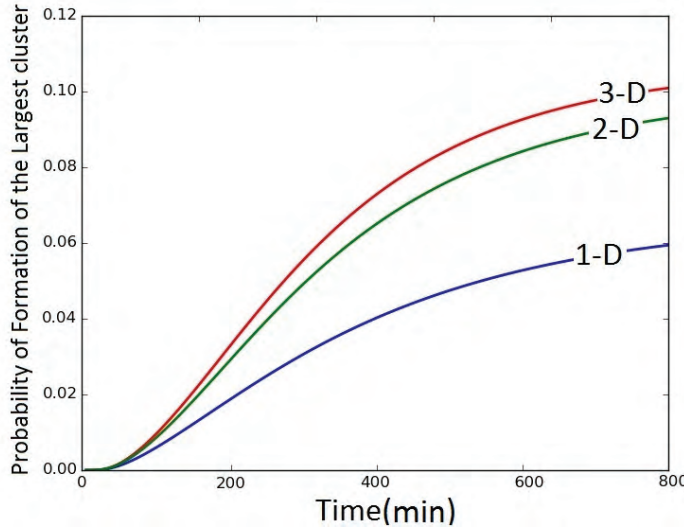


Figure 3: The probability of formation of the largest cluster at different time in different dimensions when the attachment/detachment rates ratio r is equal to 1.0. In two-dimensional/three-dimensional systems, this probability is twice that in one-dimensional systems, while the difference between two dimensional and three-dimensional systems is negligible.

Probability of forming clusters of different sizes. The formation of large clusters is an important issue in CF processes. Without loss of generality, we set a critical probability $p_{\theta,max}$ of having the largest cluster to be 0.3. Fig. 5 shows the steady-state probabilities of different clusters with different r . When $r < 3.0$, probability of having largest clusters p_{16} is less than $p_{\theta,max}$ (Fig. 5A). When this ratio is around 3, the probabilities for all clusters are almost equal to 0.3. Thus, for the assumed $p_{\theta,max}$, $r = 3.0$ is the critical ratio of attachment to detachment rate. Below this value, forming the largest cluster is unlikely.

3.3. Dynamical behavior of the CF system

To understand the time dependence of forming large clusters, we examine the time a CF system takes to reach the critical probability of $p_{\theta,max}$. Fig. 6A shows how p_{16} changes at different ratios of attachment to detachment rates. When $r < 3.0$, the probability of forming the largest cluster is less than $p_{\theta,max} = 0.3$, regardless of how much time has passed. Fig. 6B shows the

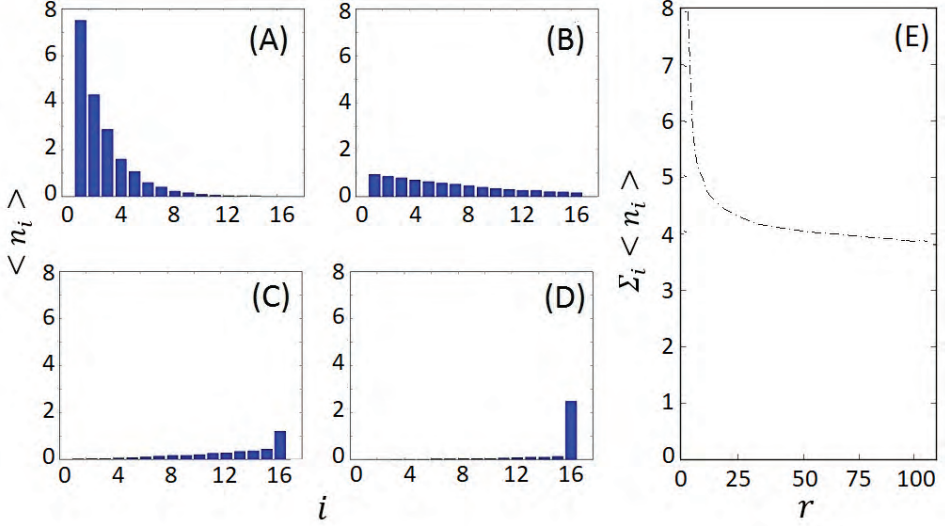


Figure 4: Expected number of clusters for different $a_{i,j}/d_{i,j}$ at steady-state: (A) $r = 0.1$, (B) $r = 1$, (C) $r = 10$, and (D) $r = 1000$. When r increases, the expected number of large particles in the system increases. (E) Expected number of clusters of all sizes in the system.

critical time at which the probability of forming the largest cluster reaches $p_{\theta,max}$ (white region). Before this critical time, formation of large clusters is unlikely to occur (blue region). A system containing large clusters is more likely after this critical time (red region). In the extreme cases, when $r > 1,000$, it is highly probable that large clusters will form within 40 minutes. In contrast, when $r \approx 3.0$, it takes about 150 minutes acquire an appreciable probability of > 0.3 of a maximum-size cluster (Fig. 6B).

We examined the convergence behavior in reaching the steady-state distribution. Table 3 lists the distance to the steady-state measured as $|p_{16}(\infty) - p_{16}(t)|$ at different times and with different r . Larger r leads to faster convergence.

Following [5], we analyzed the elasticity and sensitivity of parameters of the CF system for a subset of clusters present at different ratios of r . We use sensitivity to examine the response of the expected number of different clusters to changes in r . We use elasticity to examine the relative changes in the expected number of different clusters with respect to the relative changes in

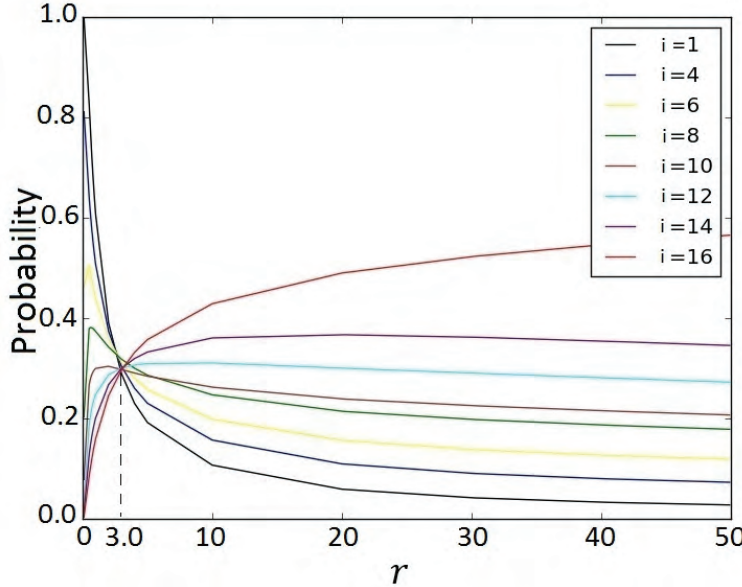


Figure 5: Probability of local clusters with size i at steady-state for different $r = a_{i,j}/d_{i,j}$. The probability of clusters with size 16 becomes more than the probability of other clusters when $r > 3$, while it is less than the probability of other clusters when $r < 3$.

in r . Following [5], the sensitivity S and the elasticity E of forming a cluster of size i are calculated as eq. 13 and eq. 14.

$$(13) \quad S(t) = \frac{\partial \langle n_i(t) \rangle}{\partial r}$$

$$(14) \quad E(t) = \frac{r}{\langle n_i(t) \rangle} \cdot \frac{\partial \langle n_i(t) \rangle}{\partial r}$$

Fig. 7 shows S and E for formation of four clusters of sizes 4, 8, 12, and 16 at three different r of 5, 20, and 50. When r increases, S and E decrease. In addition, smaller clusters have higher S and E .

3.4. Dependence on initial conditions

In the examples above, we assumed 48 particles are initially in the source which can be transformed into the system through synthesis reactions. We now examine the effect of different initial conditions on the formation of the

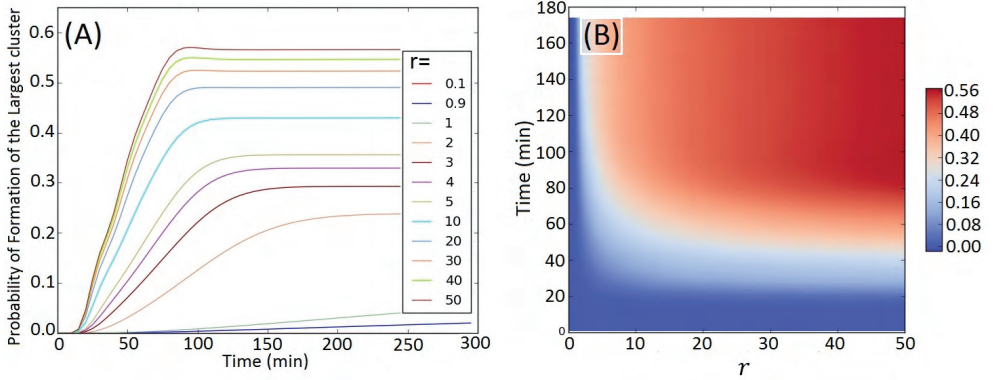


Figure 6: Time dependence of the probability to form maximum-size clusters for different ratios r of the attachment to detachment rates. (A): Probability of formation of largest cluster grows when r increases. When $a_{i,j}/d_{i,j} = 3$ probability of formation of largest cluster becomes equal to the critical probability of $p_{\theta,max} = 0.3$, after the system reaches the steady-state. (B): Critical time (white region) at which the probability of forming the largest cluster reaches $p_{\theta,max}$. Before this critical time (blue region), formation of the largest cluster is unlikely and after this critical time (red region), it is highly probable that the system contains the largest cluster.

maximum-sized clusters and the time it takes for the system to reach the steady-state.

We start with different initial conditions constrained to the same initial mean size (IMS) of clusters. Fig. 8 shows the evolutions of the probability of forming the largest cluster for four different initial conditions: 12 clusters of size 4 ($n_4 = 12$), 6 clusters of size 3 and 6 clusters of size 5 ($n_3 = 6, n_5 = 6$), 6 clusters of size 2 and 6 clusters of size 6 ($n_2 = 6, n_6 = 6$), 6 monomers and 6 clusters of size 7 ($n_1 = 6, n_7 = 6$). All these initial conditions have the same mean cluster size of 4. Overall, these systems with different initial conditions show very similar dynamics.

Figs. 9A–9B show the time-dependent behavior of the probability of forming the largest cluster under initial conditions with different IMS and $r = 3.0$ and $r = 5.0$, respectively. When $r = 3.0$ and 5.0 , the mean size of clusters at the steady-state is about 8.0 and 9.0, respectively (Fig. 4E). Fig. 9A–9B also show the time required for reaching the steady-state for

$a_{i,j}/d_{i,j}$	$ p_{16}(\infty) - p_{16}(t) $							$p_{16}(\infty)$
	t=20	t=40	t=60	t=80	t=100	t=120	t=140	
2.0	0.244	0.229	0.196	0.160	0.121	0.084	0.050	0.248
3.0	0.292	0.254	0.196	0.135	0.075	0.035	0.012	0.298
4.0	0.321	0.262	0.185	0.110	0.047	0.014	0.000	0.331
5.0	0.343	0.266	0.183	0.095	0.035	0.010	0.000	0.358
10.0	0.402	0.277	0.158	0.056	0.008	0.000	0.000	0.429
20.0	0.453	0.296	0.140	0.034	0.000	0.000	0.000	0.492
30.0	0.115	0.306	0.135	0.023	0.000	0.000	0.000	0.525
40.0	0.125	0.318	0.130	0.019	0.000	0.000	0.000	0.550
50.0	0.136	0.327	0.140	0.019	0.000	0.000	0.000	0.571

Table 3: The convergence behavior of the system at different time steps at different ratios of the attachment to detachment rates.

different IMSs. Not surprisingly, the time to approach the steady-state distribution for values of IMSs that are closer to the steady-state mean cluster sizes is less.

Figs. 9C–9D show the time required for the system to reach the steady-state for $r = 3.0$ and $r = 5.0$, respectively. Our results show that the closer the mean size of clusters at the initial condition to that of the steady-state, the less time it takes for the system to approach the stationary distribution. However, we observe that systems started at IMSs greater than the mean sizes at steady-state take longer to relax than those started at IMS smaller than at steady-state.

4. Summary and Conclusions

Coagulation and fragmentation is a fundamental process that plays an important role in many physical and biological processes. Here we studied the general properties of the CF process using the Accurate Chemical Master Equation (ACME) method [33], which can provide accurate solutions to the discrete Chemical Master Equation (dCME) and can account for the stochasticity and the discreteness of the CF process.

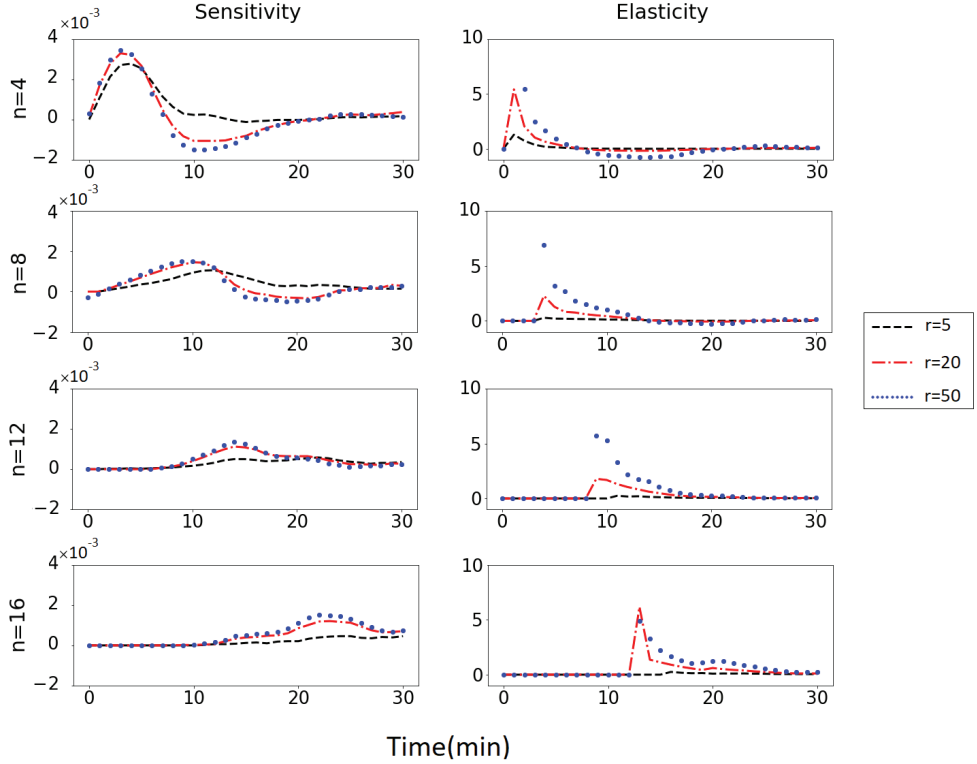


Figure 7: Sensitivity and elasticity of formation of clusters of size $N = 4, 8, 12, 16$ at different ratios of the attachment to detachment rate $r = 5, 20$, and 50 . When the size of clusters increase, sensitivity and elasticity decrease.

We examined how the dimensionality of the clusters affects their behaviors given the same intrinsic attachment and detachment rates. Three-dimensional systems exhibit faster dynamics compared to systems in one-dimension or two-dimension. This is because the dimensionality of the clusters affects the effective rates of attachment and detachment.

Steady-state probability distributions of cluster sizes were also studied under varying attachment/detachment rate ratios. For a given critical probability of emergence of maximum-sized clusters, we are able to determine the critical ratio between the attachment and detachment rates. Below this critical ratio, larger clusters of interest is unlikely to form, regardless of time. For systems with ratios larger than the critical one, we are able to calculate

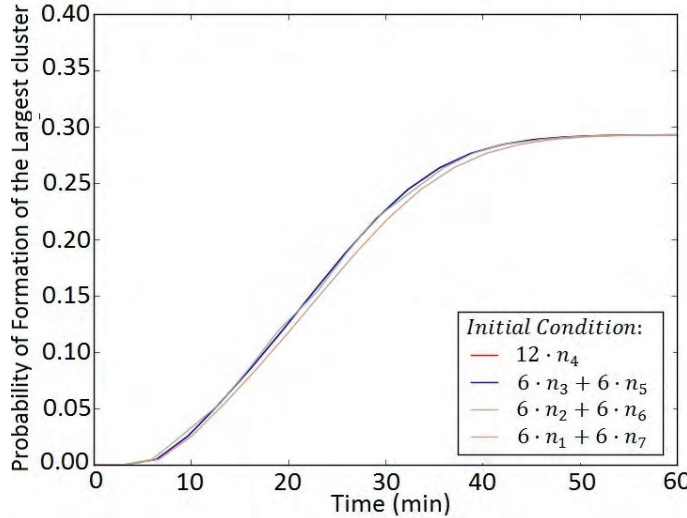


Figure 8: Probability of formation of largest cluster for different initial conditions where initial conditions have same mean cluster size. When IMSs are the same, different initial conditions show very similar dynamics

the time required for the system to form maximum-sized cluster with high probability [36, 37].

We further studied how different initial conditions affect the behavior of the system and find the initial mean size of the clusters is one of the most important factors that governs the CF dynamics. We find that the dynamics of systems started with different initial configurations but the same initial mean cluster sizes are similar. Further investigation shows that the dynamics towards steady-state are related to the deviation of the mean initial cluster size from the mean cluster size at steady-state.

Future studies include analysis of various processes of self assembly of different types of particles that occur in small closed systems, with limited supplies. Particles with different binding order and binding geometry can be explored in greater detail. An example is the HIV-1 viral capsid nucleation process [5]. In addition, critical steps of the blood-clotting processes involving fibrin and other molecules in the blood-clotting process [14] can also be studied.

Acknowledgments. JL acknowledges support from the National Institute of Health (R35GM127084, R01CA204962-01A1, and R21 AI126308).

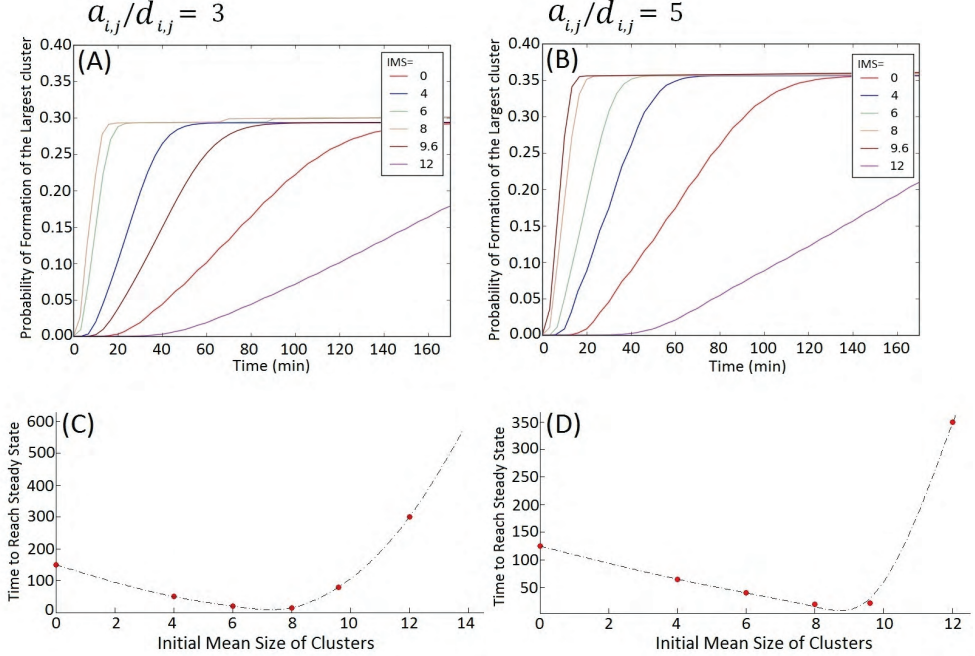


Figure 9: Probability of forming maximum-sized clusters for different initial conditions with different initial mean size of cluster. (A): $r = 3$, (B): $r = 5$, respectively; Time required for a CF system to reach steady-state for different initial conditions. (C): $r = 3$, (D): $r = 5$.

TC acknowledges support from the Army Research Office (W911NF-18-1-0345) and the National Science Foundation (DMS-1516675 and DMS-1814364).

References

- [1] S. Tsantilis and E. Pratsinis, *Evolution of primary and aggregate particle-size distributions by coagulation and sintering*, Aiche Journal **46** (2000), no. 2, 407–415.
- [2] E. Goudeli, M. L. Eggersdoref, and S. E. Pratsinis, *Coagulation–Agglomeration of fractal-like particles: Structure and self-preserving size distribution*, Langmuir **31** (2015), no. 4, 1320–1327.

- [3] H. Keramati, M. H. Saidi, and M. Zabetian, *Stabilization of the suspension of zirconia microparticle using the nanoparticle halos mechanism: Zeta potential effect*, Journal of Dispersion Science and Technology **37** (2016), no. 1, 6–13.
- [4] D. Sept and J. A. McCammon, *Thermodynamics and kinetics of actin filament nucleation*, Biophysical Journal **81** (2001), no. 2, 667–674.
- [5] Farrah Sadre-Marandi, Yuewu Liu, Jiangguo Liu, Simon Tavener, and Xiufen Zou, *Modeling HIV-1 viral capsid nucleation by dynamic systems*, Mathematical Biosciences **270** (2015), 95–105.
- [6] E. T. Powers and D. L. Powers, *The kinetics of nucleated polymerizations at high concentration: Amyloid fibril formation near and above the super critical concentration*, Biophysical Journal **91** (2006), 122–132.
- [7] L. Edelstein-Keshet and G. Bard Ermentrout, *Models for the length distributions of actin filaments: I. Simple polymerization and fragmentation*, Bulletin of Mathematical Biology **60** (1998).
- [8] A. T. Nurden, *The biology of the platelet with special reference to inflammation, wound healing and immunity*, Frontiers in Bioscience **23** (2018), 726–751.
- [9] M. Bertsch, B. Franchi, N. Marcello, M. C. Tesi, and A. Tosin, *Alzheimer’s disease: A mathematical model for onset and progression, mathematical medicine and biology*, Italian Ministry of Health **34** (2017), no. 2, 193–214.
- [10] A. K. Tarbox and M. Swaroop, *Pulmonary embolism*, International Journal of Critical Illness and Injury Science, **3** (2013), no. 1, 69–72.
- [11] B. Englemann, *Initiation of coagulation by tissue factor carriers in blood*, Blood Cells, Molecules, and Diseases **36** (2006), 188–190.
- [12] M. F. Hockin, K. C. Jones, S. J. Everse, and K. G. Mann, *A model for the stoichiometric regulation of blood coagulation*, The Journal of Biological Chemistry **227** (2002), no. 21, 18322–18333.
- [13] M. S. Chatterjee, W. S. Denney, H. Jing, and S. L. Diamond, *System biology of coagulation initiation: Kinetics of thrombin generation in resting and activated human blood*, PLOS Computational Biology **6** (2010), no. 9, e1000950.
- [14] R. D. Guy, A. L. Fogelson, and J. P. Keener, *Fibrin gel formation in a shear flow*, Mathematical Medicine and Biology **0** (2005), 1–20.

- [15] P. L. Krapivsky and S. Redner, and E. Ben-Naim, *A Kinetic View of Statistical Physics*, Cambridge University Press, Cambridge, UK, 2010.
- [16] R. M. Ziff and G. Stell, *Kinetics of polymer gelation*, The Journal of Chemical Physics **73** (1980), no. 7, 3792.
- [17] J. A. D. Wattis and J. R. King, *Asymptotic solutions of the Becker-Döring*, Journal of Physics A: Mathematical General **31** (1998), 7169–9189.
- [18] W. M. Mounts, M. N. Liebman, *Qualitative modeling of normal blood coagulation and its pathological states using stochastic activity networks*, International Journal of Biological Macromolecules **20** (1997), 265–281.
- [19] N. Hoze and D. Holcman, *Stochastic coagulation-fragmentation processes with a finite number of particles and applications*, Annals of Applied Probability **28** (2016), no. 3, 1449–1490.
- [20] B. Niethammer, *On the evolution of large clusters in the Becker-Döring model*, Journal of Nonlinear Science **13** (2003), no. 1, 115–155.
- [21] O. Penrose, *The Becker-Döring equations at large times and their connection with the LSW theory of coarsening*, Journal of Statistical Physics **89** (1997), no. 1-2, 305–320.
- [22] J. K. Davis and S. S. Sindi, *Initial condition of stochastic self-assembly*, Physical Review E **93** (2016), no. 2, 022109.
- [23] A. Gupta, J. Mikelson, and M. Khammash, *A finite state projection algorithm for the stationary solution of the chemical master equation*, The Journal of Chemical Physics **147** (2017), 154101.
- [24] V. Sudbrack, L. G. Brunnet, R. M. C. de Almeida, R. M. Ferreira, and D. Gamermann, *Master equation for degree distribution of a duplication and divergence network*, Physica A **509** (2015), 588–298.
- [25] P. Smadbeck and Y. N. Kaznessis, *Solution of chemical master equations for nonlinear stochastic reaction networks*, Current Opinion in Chemical Engineering **5** (2014), 90–95.
- [26] Y. Cao and J. Liang, *Adaptively biased sequential importance sampling for rare events in reaction networks with comparison to exact solution from finite buffer dCME method*, The Journal of Chemical Physics **139** (2013), no. 2, 025101.

- [27] A. Terebus, Y. Cao, and J. Liang, *Exact computation of probability landscape of stochastic networks of single input and coupled toggle switch modules*, IEEE Engineering in Medicine and Biology Society (EMBS) **2014** (2014), 5228–5231.
- [28] Y. Cao, A. Terebus, and J. Liang, *State space truncation with quantified errors for accurate solution to discrete chemical master equation*, Bulletin of Mathematical Biology **78** (2016), no. 4, 617–661.
- [29] M. R. D’Orsogna, G. Lakatos, and T. Chou, *Stochastic self-assembly of incommensurate clusters*, The Journal of Chemical Physics **136** (2012), 0884110.
- [30] M. R. D’Orsogna, Q. Lei, and T. Chou, *First assembly times and equilibrium in stochastic coagulation-fragmentation*, The Journal of Chemical Physics **143** (2015), 014112.
- [31] G. Kotalczyk and F. E. Kruis, *A Monte Carlo method for the simulation of coagulation and nucleation based on weighted particles and the concepts of stochastic resolution and merging*, Journal of Computational Physics **340** (2017), 276–296.
- [32] A. J. Smith, C. G. Wells, and M. Kraft, *A new iterative scheme for solving the discrete smoluchowski equation*, Journal of Computational Physics **352** (2018), 373–387.
- [33] Y. Cao, A. Terebus, and J. Liang, *Accurate chemical master equation solution using multi-finite buffers*, SIAM Multiscale Modeling and Simulation **14** (2016), no. 2, 923–963.
- [34] Y. Cao and J. Liang, *Optimal enumeration of state space of finitely buffered stochastic molecular networks and exact computation of steady state landscape probability*, BMC Systems Biology **2** (2008), no. 30, 1–13.
- [35] Y. Cao, A. Terebus, and J. Liang, *Chapter 3. Modeling stochastic gene regulatory networks using direct solutions of chemical master equation and rare event sampling*, in: Research in Analysis and Modeling of Gene Regulatory Networks, Ivanov Ivan V., Qian Xiaoning and Pal Ranadip. Advance in Medical Technologies and Clinical Practice (AMTCP), Book Series 2016.
- [36] T. Chou and M. R. D’Orsogna, *First passage problems in biology*, in Chapter 13: First-Passage Phenomena and Their Applications, editors R. Metzler, G. Oshanin, and S. Redner, World Scientific, 2014

- [37] R. Yvinec and M. R. D'Orsogna, and T. Chou, *First passage times in homogeneous nucleation and self-assembly*, The Journal of Chemical Physics **137** (2012), 244107.

FARID MANUCHEHRFAR¹, WEI TIAN¹, TOM CHOU², AND JIE LIANG^{1,*}

1. DEPARTMENT OF BIOENGINEERING
UNIVERSITY OF ILLINOIS AT CHICAGO (UIC)
CHICAGO, ILLINOIS, USA

2. DEPARTMENTS OF BIOMATHEMATICS AND MATHEMATICS
UNIVERSITY OF CALIFORNIA AT LOS ANGELES (UCLA)
LOS ANGELES, CALIFORNIA, USA

* CORRESPONDING AUTHOR. *E-mail address:* jliang@uic.edu

